ISSN: 1410-8917
Jurnal Kimia Sains & Aplikasi
e-ISSN: 2597-9914

Jurnal Kimia Sains dan Aplikasi 27 (6) (2024): 271-279

Jurnal Kimia Sains dan Aplikasi
Journal of Scientific and Applied Chemistry

Journal homepage: http://ejournal.undip.ac.id/index.php/ksa

Synthesis and Characterization of Silica-Biochar Composite as Rhodamine B Dye Adsorbent

Lisa Sari [1], Anis Shofiyani [1,*], Ajuk Sapar [1]

[1] Department of Chemistry, Faculty of Mathematics and Natural Sciences, Tanjungpura University, Pontianak, Indonesia

* Corresponding author: anis.shofiyani@chemistry.untan.ac.id

https://doi.org/10.14710/jksa.27.6.271-279

Article Info

Article history:

Received: 20th February 2024
Revised: 17th May 2024
Accepted: 28th May 2024
Online: 30th June 2024

Keywords:
Silica; biochar; composite; adsorption; rhodamine B

Abstract

Composites are synthesized by combining different materials, resulting in properties suitable for use as adsorbents due to the combination of pores and functional groups within the constituent materials. This study developed a silica-biochar composite to serve as an adsorbent for rhodamine B dye, utilizing silica derived from red mud and biochar obtained from oil palm empty fruit bunches (OPEFB). This research focused on analyzing the characteristics and effectiveness of the composite as an adsorbent by varying its composition. Silica from red mud exhibited a purity of 80.05% and possessed silanol (Si-OH) and siloxane (Si-O-Si) functional groups on its surface, whereas biochar from OPEFB had a carbon content of 95.91% and included functional groups such as -OH, C=O, C=C, C-H, and C-O. The combination of silica and biochar yielded a composite surface consisting of -OH, C=O, C=C, C-O, C-H, and Si-O-Si functional groups. The silica-biochar composite demonstrated a greater surface area than its individual components, with silica at 69.824 m^2/g and biochar at 95.452 m^2/g. The composite with a 1:2 (% w/w) ratio exhibited the largest surface area at 102.371 m^2/g, achieving a maximum adsorption capacity of 1.550 mg/g and an efficiency of 88.463%. The adsorption process encompasses physical interactions via pore diffusion and chemical interactions through functional groups.

1. Introduction

Silica is a porous solid formed through the polymerization of silicic acid, and it can be synthesized via the precipitation method using NaOH as a solvent and HCl as a precipitator. Red mud, which contains 3-50% silica, serves as a viable raw material for this synthesis [1]. However, silica's adsorption capacity is limited and does not correlate directly with the number of silanol (Si-OH) and siloxane (Si-O-Si) groups on its surface. Biochar can be incorporated to enhance the adsorption capacity of silica. Biochar is produced from empty palm oil bunches through dehydration and carbonization processes at high temperatures [2].

Both biochar and silica have their respective weaknesses, but combining them into a composite offers distinct advantages. Biochar's heterogeneous structures and properties result in suboptimal adsorption and anti-interference capabilities [3]. To address these limitations, researchers are exploring the formation of composite materials using silica and biochar. Nano-sized silica, known for its high specific surface area and hydrothermal stability, enhances the physicochemical properties of biochar when combined. This combination significantly improves the adsorption capacity of the resulting composite materials [4].

Silica and biochar composites have demonstrated substantial adsorption capacities, which are attributed to their enhanced specific surface area, porosity, and abundance of active groups. Research by Wang *et al.* [5] indicates that composites derived from silica (fly ash) and biochar (rice straw) possessed a larger surface area compared to the individual materials. Specifically, the incorporation of silica increased the specific surface area of rice straw-based biochar from 305 m^2/g to 330.8 m^2/g and changed the porosity from 2.8 nm to 3.1 nm. These composites exhibit silanol and siloxane groups on their surfaces and other functional groups such as C=O, C=C, C- O, and C-H. The proliferation of active groups on the

adsorbent surface can significantly enhance adsorption capacity [6]. Further research by Zhao *et al.* [7] found that adding silica to biochar facilitates the opening of micropores and the expansion of mesopores, thereby increasing the total pore volume and average pore diameter of the composite. This modification is advantageous for adsorption, particularly for binding larger molecules such as dyes.

One notable application of the silica-biochar composite is as an adsorbent. Research by Ahmad *et al.* [3] confirmed that adding silica to biochar significantly enhances its removal efficiency for chlortetracycline, achieving a 68% removal rate compared to 36% with pure biochar. Additionally, Wang *et al.* [5] demonstrated the composite's efficacy in adsorbing methylene blue dye, attributing this to the composite's large surface area and porosity. The adsorption process for methylene blue follows the Langmuir adsorption isotherm, with a maximum adsorption capacity of 131.58 mg/g.

Building on this research, a silica-biochar composite derived from red mud and empty oil palm fruit bunches was developed as an adsorbent for rhodamine B dye. The structural similarities between rhodamine B and methylene blue suggest the composite can adsorb rhodamine B through physical and chemical mechanisms. Moreover, since rhodamine B is classified as a carcinogenic waste, it must be processed through adsorption tests to ensure effective removal.

The silica-biochar composite is anticipated to be an effective adsorbent for rhodamine B dye due to its combination of pores, surface area, and functional groups capable of adsorbing the dye. The adsorption process is believed to involve several functional groups, including silanol, siloxane, hydroxyl, and carbonyl groups. The composite and rhodamine B interaction is expected to occur through both physical and chemical adsorption mechanisms. Physical adsorption leverages the pores of the silica and biochar, while chemical adsorption involves the functional groups through electrostatic interactions, hydrogen bonds, and covalent bonds [8].

The composition ratio of silica to biochar significantly influences the characteristics and adsorption capacity of the composite. Research by Zhao *et al.* [7] indicated that increasing the amount of silica can occlude the pore cavities of the biochar, thereby reducing the overall surface area and adsorption capacity of the composite. This study examined the effectiveness of the composite as an adsorbent by analyzing the effect of the silica-biochar composition ratio on the adsorption of rhodamine B.

2. Experimental

2.1. Tools and Materials

The tools used were a 100-mesh sieve, hot plate, filter paper, porcelain crucible, analytical balance, oven, pH meter (Hanna-HI110), Scanning Electron Microscopy -Energy Dispersive X-Ray (SEM-EDX) JEOL JSM-6510LA, set of reflux tools, shaker, Fourier Transform Infra-Red spectrophotometer (FTIR) Shimadzu IR Prestige 21, UV-Vis spectrophotometer Shimadzu UV-2600, furnace, X-ray Diffraction (XRD) X'pert PRO PANalytical and X-ray Fluorescence (XRF) PANalytical Epsilon 3. The materials used were distilled water, 37% hydrochloric acid (Merck), methylene blue (Merck), sodium hydroxide (Merck), and red mud obtained from PT. Indonesia Chemical Alumina (ICA) West Kalimantan, rhodamine B, and oil palm empty fruit bunch (OPEFB).

2.2. Synthesis of Silica from Red Mud

A total of 100 g of neutral red mud was reacted with 250 mL of 4 M NaOH solution. The mixture was refluxed until boiling while being stirred at 650 rpm, and the reaction was maintained for 120 minutes. The resulting mixture was then filtered, and the filtrate was gradually added to a 1 M HCl solution until a gel formed at a pH of 6.5 to 7. The silicic acid gel was aged 24 hours, filtered, and washed with distilled water. Subsequently, the silica gel was dried at 110°C for 6 hours, crushed, and sieved through a 100-mesh sieve [9].

2.3. Biochar Production from Oil Palm Empty Fruit Bunches

Oil palm empty fruit bunches were washed with clean water and dried until they reached a constant weight. The dried OPEFB was then ground into a powder and burned in a furnace at 400°C for 1 hour. The resulting biochar was crushed to a fine consistency and sieved through a 100-mesh sieve. The yield of biochar was calculated using Equation (1).

$$\%\ yield = \frac{biochar\ mass}{OPEFB\ mass} \times 100\% \quad (1)$$

A proximate analysis of the biochar, including the determination of water content and ash content, was conducted according to the procedure outlined in SNI 06-3730-1995.

2.4. Determination of Water Content

A total of 1 g of biochar was placed into a tared porcelain crucible. The biochar was then placed in an oven at 110°C for 3 hours, followed by cooling in a desiccator for 15 minutes and subsequent weighing. This process was repeated, with the biochar being reheated in the oven every hour at 110°C until a constant weight was obtained. The water content of the biochar was calculated using Equation (2).

$$Water\ content\ (\%) = \frac{(m_1 - m_2)}{m_1} \times 100\% \quad (2)$$

where, m_1 is the mass of the initial sample (biochar) (g), and m_2 is the mass of the final sample (g).

2.5. Determination of Ash Content

A total of 2 g of biochar was placed into a tared porcelain crucible. The biochar was heated in a furnace at 800°C for 2 hours, allowed to cool in a desiccator for 15 minutes, and then weighed. This process was repeated several times until a constant weight was achieved. The ash content in the biochar was determined using Equation (3).

$$Ash\ content\ (\%) = \frac{m_1}{m_2} \times 100\% \quad (3)$$

where, m_1 is the initial sample mass (g) and m_2 is the ash mass after kiln (g).

2.6. Synthesis and Characterization of Silica-Biochar Composite

Composites were prepared with varying silica ratios to biochar: 1:2, 1:1, and 2:1 (% w/w). The two components were mixed together, and 100 mL of distilled water was added to facilitate homogenization. The mixture was stirred using a magnetic stirrer for 2 hours and then filtered. The resulting solid was subsequently dried at 110°C for 6 hours [5]. The composite materials were characterized using an FTIR spectrophotometer. Additionally, the composite with a ratio of 1:2 (% w/w) was further analyzed using SEM-EDX analysis. For comparison, characterization was also performed on the silica and biochar individual materials.

2.7. Surface Area Determination Based on Methylene Blue Adsorption

This procedure was based on the study conducted by Mulyati [10] with some modifications. Specifically, 0.01 g of the adsorbent was mixed with 20 mL of a 20 ppm methylene blue solution. The mixture was stirred at 150 rpm for 120 minutes using a shaker. Subsequently, the mixture was filtered, and the absorbance of the resulting filtrate was measured at a wavelength of 664 nm. The surface area of the adsorbent was assessed using Equation (4), while the amount of methylene blue adsorbed (X_m) was determined using Equation (5).

$$\text{Surface area } (m^2/g) = \frac{X_m \times N \times A}{M_r} \quad (4)$$

where N is Avogadro's number (6.02×10^{23} molecules/mol), A is the cross-sectional area of methylene blue (197×10^{-20} m^2/molecule), and Mr is the relative molecular mass of methylene blue (320.5 g/mol).

2.8. Adsorption of Rhodamine B on Silica-Biochar Composite

This experimental procedure was based on the methodology described by Haryono *et al.* [11], with modifications. Each sample containing 0.25 g of the control and silica-biochar composites, with mass ratios of 1:2, 1:1, and 2:1 (% w/w), was introduced into a 20 ppm rhodamine B solution. The mixture was agitated using a shaker at 150 rpm for 120 minutes to facilitate adsorption. Subsequently, the mixture was filtered, and the absorbance of the filtrate was measured at a wavelength of 554 nm. The amount of rhodamine B adsorbed and the percentage adsorption efficiency were calculated using Equations (5) and (6), respectively.

$$X_m = \frac{C_0 - C_1}{W} \times V \quad (5)$$

$$\%E_p = \frac{C_0 - C_1}{C_0} \times 100\% \quad (6)$$

where X_m is the amount of adsorbate adsorbed (mg/g), C_0 is the initial concentration (mg/L), C_1 is the final concentration (mg/L), V is the solution volume (mL), W is the mass of the adsorbent (g), and Ep is the adsorption efficiency (%).

3. Results and Discussion

3.1. Silica from Red Mud

The synthesis of silica from red mud involves dissolving SiO_2 using a 4 M NaOH solution. This process yields a sodium silicate solution, serving as a silica gel formation precursor. The sodium silicate is then reacted with a 1 M HCl solution as a precipitant to produce a solid silicic acid gel (H_2SiO_3). Subsequently, the gel undergoes a maturation process (aging), forming a stiffer polymer network and experiencing volume shrinkage. The addition of HCl generates salt compounds, which are removed by washing with distilled water. Heating the precipitate reduces the size of the silica gel due to the dehydration of silicic acid, resulting in the formation of silica (SiO_2) and the release of water molecules [12]. The final product of synthesis is white silica powder. The mechanism of silica formation could be described by Equation (7) to (9).

$$SiO_{2(s)} + 2NaOH_{(aq)} \rightarrow Na_2SiO_{3(aq)} + H_2O_{(aq)} \quad (7)$$

$$Na_2SiO_{3(aq)} + 2HCl_{(aq)} \rightarrow H_2SiO_{3(s)} + 2NaCl_{(aq)} \quad (8)$$

$$H_2SiO_{3(s)} \rightarrow SiO_{2(s)} + H_2O_{(g)} \quad (9)$$

The purity of the synthesized silica is determined through XRF analysis. As shown in Table 1, the silica composition of red mud increased from 9.05% to 85.05% after the synthesis stage. The resulting silica exhibits a purity of 85.05%, though it still contains minor impurities at lower percentages.

Table 1. Composition of elements and oxide compounds in red mud and silica

% Relative weight					
Element	Red mud	Silica	Oxide compound	Red mud	Silica
Fe	81.34	1.50	Fe_2O_3	75.14	0.65
Si	5.55	83.05	SiO_2	9.05	85.05
Al	5.95	9.60	Al_2O_3	8.05	11.00
Ti	3.14	0.13	TiO_2	3.72	0.07
Ca	2.62	1.80	CaO	2.61	0.80
P	0.30	2.20	P_2O_5	0.45	1.75
K	0.22	0.45	K_2O	0.20	0.17
Other	0.88	1.27	Other	0.78	0.51

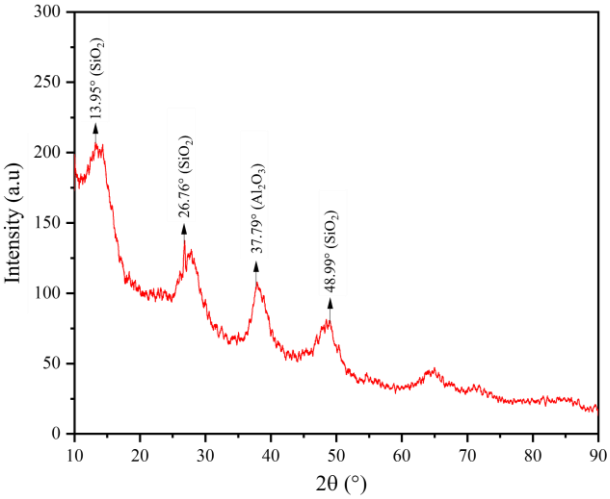

Figure 1. Silica diffractogram

Characterization using XRD aims to determine the phases formed in silica. The diffractogram in Figure 1 shows the appearance of the quartz phase at the corners 2θ = 26.76° (ICDD No. 01-083-2466) and the cristobalite phase at corner 2θ = 13.95° and 48.99° (ICDD No. 01-082-1576 and ICDD No. 00-047-1301). Apart from silica, the presence of alumina minerals (Al_2O_3) with a corundum phase was detected at an angle of 2θ = 37.79° (ICDD No. 01-077-2135). Alumina minerals are not completely lost during the synthesis process.

Figure 2 depicts that the FTIR spectrum of red mud exhibits several peaks corresponding to the vibrations of -OH, Si-O-R (R: Si or Al), and Fe-O groups. This is due to the composition of red mud, which includes various inorganic compounds such as silica, alumina, and iron oxide. In contrast, the FTIR spectrum of silica is dominated by the presence of silanol (Si-OH) and siloxane (Si-O-Si) functional groups, which are characteristic of the silica framework. The broadened peaks at 3421.72 cm^{-1} and 3452.58 cm^{-1} indicate the presence of -OH stretching vibrations from the gibbsite [13], as well as silanol groups (Si-OH) [14]. The presence of the -OH group is further confirmed in each spectrum by the absorption peak at 1647.21 cm^{-1}. This absorption indicates the bending vibration of the -OH group from water molecules [15] and the Si-OH group [14].

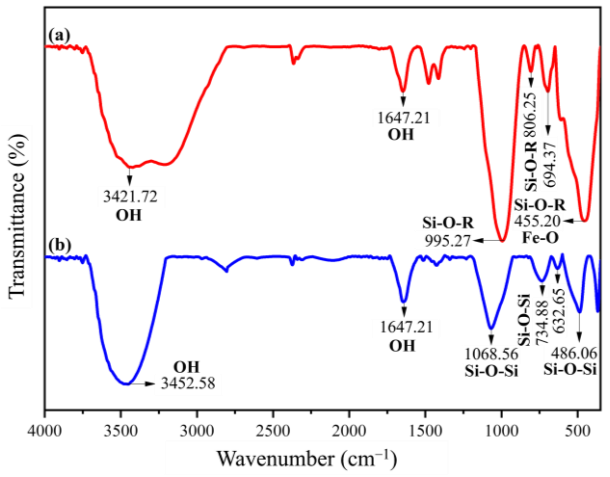

Figure 2. FTIR spectra of (a) red mud and (b) silica

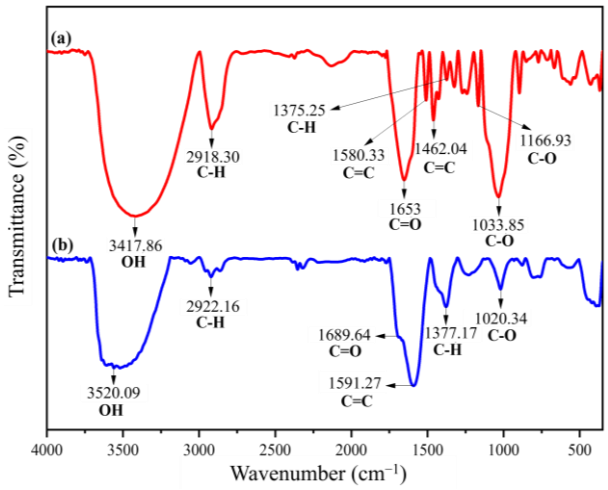

Figure 3. FTIR spectra of (a) OPEFB and (b) biochar

The symmetric and asymmetric stretching vibrations of Si-O-R (R: Si or Al) in the tetrahedral framework $[SiO_4]$ or $[AlO_4]^-$ are identified by absorptions at 806.25 cm^{-1}, 694.37 cm^{-1} [16], and 995.27 cm^{-1} [17]. Additionally, the absorption at 455.20 cm^{-1} corresponds to the bending vibration of Si-O-R [15] and the Fe-O bond in hematite and magnetite compounds [18]. The FTIR spectrum of silica reveals the presence of symmetric and asymmetric stretching vibrations of siloxane (Si-O-Si) at absorptions of 734.88 cm^{-1}, 632.65 cm^{-1}, and 1068.56 cm^{-1}. The bending vibrations of Si-O-Si occur at the absorption of 486.06 cm^{-1} [19].

3.2. Biochar from Oil Palm Empty Fruit Bunches

Biochar from OPEFB raw materials is produced through pyrolysis, an incomplete combustion reaction. During pyrolysis, the water in OPEFB evaporates at temperatures between 100 and 200°C, followed by the decomposition of organic materials such as hemicellulose (200–350°C), cellulose (305–375°C), and lignin (250–500°C) [20]. The resulting product is black biochar, with a yield of 36%.

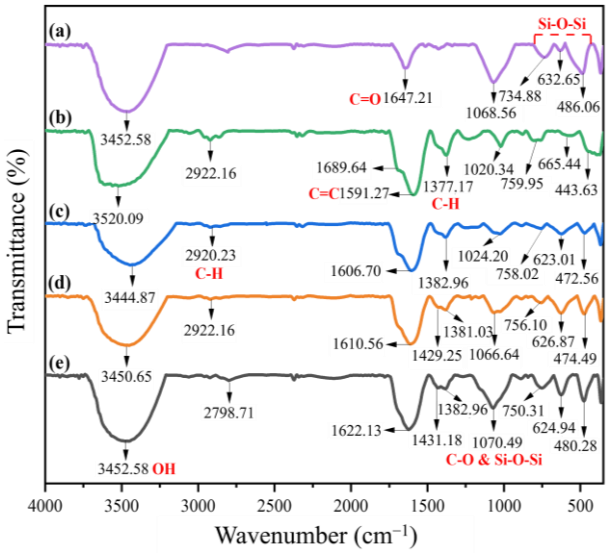

Figure 4. FTIR spectra of (a) silica, (b) biochar, (c) silica-biochar composite variations 1: 2 (% w/w), (d) 1: 1 (%w/w), and (e) 2: 1 (% w/w)

Table 2. Results of proximate analysis of biochar from oil palm empty fruit bunches

Analysis parameter	Biochar	SNI 06-3730-1995
Water content (%)	6.13	Max. 15
Ash content (%)	7.50	Max. 10

Table 2 presents the water content (6.13%) and ash content (7.50%) of biochar, which comply with SNI 06-3730-1995 standards. Biochar with low water and ash content exhibits superior adsorption capabilities, as the absence of water molecules and mineral residues ensures that more pores remain available to adsorbate [21].

The FTIR spectra in Figure 3 show broadening peaks at 3417.86 cm^{-1} and 3520.09 cm^{-1}, corresponding to the - OH stretching vibrations of phenol and alcohol groups. The absorption intensity of the -OH group decreases after conversion to biochar due to the dehydration of alcohol [2]. The absorptions at 2918.30 cm^{-1} (OPEFB) and 2922.16 cm^{-1} (biochar) are associated with aliphatic C-H stretching vibrations in the lignocellulosic framework [22]. The stretching vibrations of the conjugated C=O of carboxyl and ketone groups appear at absorptions of 1653.00 cm^{-1} (OPEFB) and 1689.64 cm^{-1} (biochar). The absorption intensity of the C=O group decreases after the conversion to biochar. The absorption peak in the range of 1591.27–1462.04 cm^{-1} is associated with aromatic C=C stretching vibrations [2]. Absorptions at 1375.25 cm^{-1} (OPEFB) and 1377.17 cm^{-1} (biochar) indicate the presence of aliphatic C-H bending vibrations from cellulose and hemicellulose [23], while the absorption range of 1166.93–1020.34 cm^{-1} corresponds to the C-O stretching vibrations from ether and alcohol functional groups [24].

Figure 3 demonstrates that pyrolysis effectively removes most cellulose and hemicellulose from OPEFB, leaving lignin compounds behind. This is evidenced by the decrease in absorption intensity of functional groups containing oxygen and C-H groups, alongside an increase in the absorption intensity of C=C functional groups on the biochar surface [2]. The presence of the C=C functional group is characteristic of the lignin structure [25]. According to Chen *et al.* [26], lignin is a large polymer with a three-dimensional structure and is composed of phenylpropane structural units. The chemical structure of lignin is notably stable compared to cellulose and hemicellulose, requiring high temperatures and extended pyrolysis times for complete decomposition.

Table 3. Results of determining methylene blue adsorption and adsorbent surface area

Adsorbent	C1 (mg/L)	C absorbed (mg/L)	X_m (mg/g)	S (m^2/g)
Control				
Silica	5.082	9.435	18.870	69.824
Biochar	1.619	12.898	25.796	95.452
Silica-Biochar composite				
1: 2	0.684	13.833	27.666	102.371
1: 1	0.729	13.788	27.576	102.038
2: 1	0.799	13.718	27.436	101.520

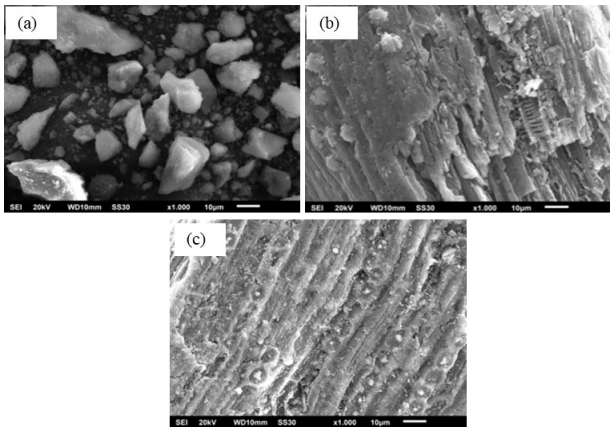

Figure 5. SEM analysis results with 1000× magnification of (a) silica, (b) biochar, and (c) silica-biochar composite 1: 2 (% w/w)

3.3. Silica-Biochar Composite

The determination of surface area is essential for assessing the physical characteristics of each adsorbent, as the adsorption capacity is influenced by the available surface area. Table 3 shows the quantity of methylene blue molecules absorbed correlates directly with the greater surface area of the adsorbent. This is attributed to the larger surface area providing more contact sites that can be occupied by methylene blue [27]. In comparison, biochar exhibits a larger surface area than silica, specifically 95.452 m^2/g and 69.824 m^2/g, respectively. Increasing the proportion of silica in composite synthesis results in a reduction of surface area. The silica: biochar composite with the highest surface area is observed in the 1:2 (%w/w) variation, amounting to 102.371 m^2/g.

Figure 4 displays spectra of silica, biochar, and composites characterized by peaks with varying absorption intensities influenced by the composition of silica and biochar during composite production. Each spectrum in the composite exhibits a broad absorption peak in the range of 3452.58–3444.87 cm^{-1}, attributed to the stretching vibration of the -OH group [5]. The absorption peaks in the ranges of 2922.16–2798.71 cm^{-1} and 1622.13–1606.70 cm^{-1} correspond to C-H stretching and C=O stretching vibrations of ketones and carboxyls, respectively [28].

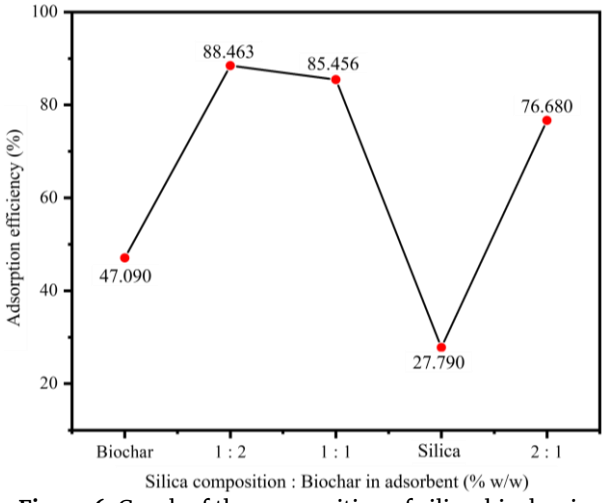

Figure 6. Graph of the composition of silica: biochar in the adsorbent vs. % adsorption efficiency

Table 4. EDX analysis results of biochar and silica-biochar composite

% Relative weight of elemental composition		
Element	Biochar	Silica-Biochar Composite
C	95.91	94.19
O	1.84	1.90
Si	1.31	0.36
Al	0.14	0.64
Na	0.20	-
Other	0.60	2.91

In biochar, the absorption peak at 1591.27 cm^{-1}, representing the C=C stretching vibration of the aromatic ring, shifts to a lower wavenumber (1431.18–1429.25 cm^{-1}) after the addition of silica [2]. According to Ahmad *et al.* [28], this shift in wavenumber in the FTIR spectrum indicates an interaction between SiO_2 and biochar during composite formation. Each spectrum also exhibits an absorption at 1382.96–1381.03 cm^{-1}, associated with C-H bending vibrations [23]. The absorption in the range of 1070.49–1024.20 cm^{-1} corresponds to the C-O stretching vibration of the ether functional group [28] and the Si-O-Si stretching vibration [29]. The presence of the Si-O-Si functional group is confirmed by absorptions in the range of 758.02–472.56 cm^{-1} [28].

Adding silica to biochar enhances the availability of oxygen-containing functional groups and reduces the absorption intensity of C=C functional groups on the composite surface. The absorption intensity of the -OH and Si-O-Si groups increases with higher silica composition in each spectrum. This indicates that silica has been successfully incorporated into the biochar surface [8].

Figure 5a illustrates that the silica surface contains particles that tend to form non-uniform clusters, likely due to the aggregation of silica particles with other components not separated during synthesis [30]. Figure 5b shows that biochar has a rough surface. The addition of silica to biochar results in a smoother surface morphology, as depicted in Figure 5c. Some composite pores appear to be covered by particles presumed to be silica. Similar findings were reported by Wang *et al.* [5], where silica-biochar composites exhibited surfaces covered with coarse particles. EDX analysis results in Table 4 indicate that the biochar surface is predominantly composed of carbon. Adding silica to the biochar decreases the carbon content from 95.91% to 94.19%.

3.4. Adsorption of Rhodamine B on Silica-Biochar Composite

A calibration curve yielded a linear equation y = 0.091x -0.0041 with an R^2 value of 0.9998. The adsorption of rhodamine B was conducted using the batch method, involving mixing a fixed amount of the composite with rhodamine B. Figure 6 shows that as the silica content on the adsorbent's surface decreases, the concentration of absorbed rhodamine B increases. The adsorption capacity is linked to the surface area, with the composite adsorbing more rhodamine B than silica or biochar alone.

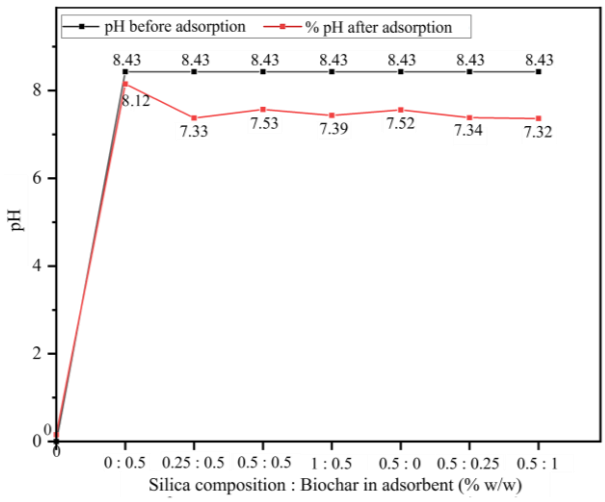

Figure 7. Graph of pH changes before and after adsorption

The amount of rhodamine B adsorbed decreased with increasing silica composition. This occurs because larger amounts of silica can cover the pore cavities of biochar, thereby reducing the contact surface available for rhodamine B and its adsorption efficiency [7]. The composite variation 1:2 (%w/w) adsorbed the greatest amount of rhodamine B, with an adsorption capacity of 1.550 mg/g and an adsorption efficiency of 88.463%.

The adsorption of rhodamine B involves both physical and chemical interactions. Physical interactions are characterized by the adsorption of rhodamine B molecules into the pores, while chemical interactions involve the functional groups on the surface of the composite and control adsorbents. The process is predominantly driven by chemical interactions, primarily due to the presence of H^+ ions released into the adsorption system. This release of H^+ ions was confirmed by analyzing the pH levels before and after adsorption. As shown in Figure 7, the pH after adsorption tends to be lower than before adsorption.

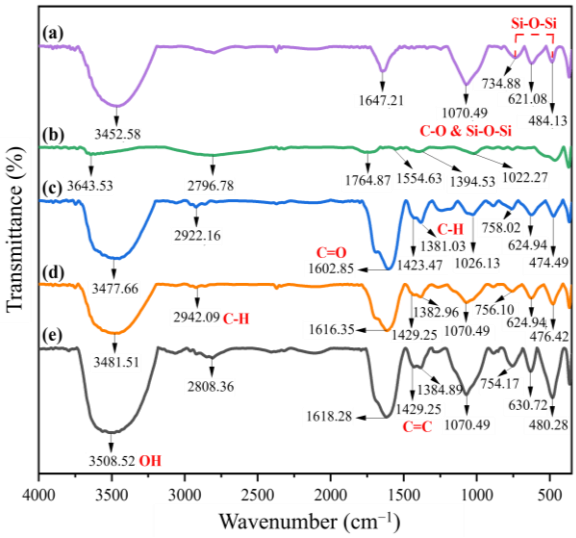

Figure 8. FTIR spectra after adsorption of (a) silica, (b) biochar, (c) silica-biochar composite variations 1: 2 (%w/w), 1: 1 (%w/w) (d), and (e) 2: 1 (%w/w)

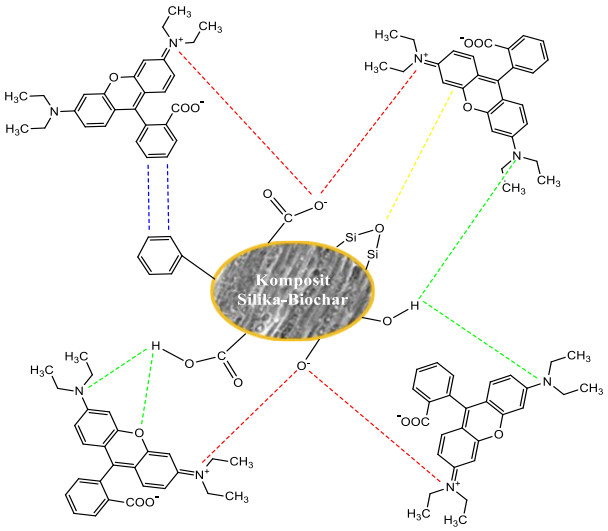

Figure 9. Estimated interaction mechanisms involved in the adsorption of rhodamine B on silica-biochar composites (--- electrostatic interactions), (--- hydrogen bonds), (--- n interactions $-\pi$) and (--- interaction $\pi-\pi$)

Rhodamine B has a pKa value of 3.1; when the pH exceeds 3.1, the rhodamine B molecule forms a zwitterion, characterized by an ionized carboxyl group (COO^-) and a cationic amino group (NH^+) [31]. The adsorption of rhodamine B occurs under alkaline conditions (pH > 7), causing some functional groups on the surface of the composite, such as -OH and COOH, to ionize to O^- and COO^-. These ionized groups repel the COO^- and attract the N^+ in the rhodamine B molecule through electrostatic interactions [2].

The spectra after adsorption (Figure 8) reveal shifts in wavenumbers corresponding to the -OH, C-H, C=O, C=C, C-O, and Si-O-Si functional groups. These shifts indicate that each functional group acts as an active site for the adsorption of rhodamine B. The shift in wave numbers for the -OH and C-O functional groups supports the hypothesis of electrostatic interactions between rhodamine B and the silica-biochar composite and the control (biochar). Also, hydrogen bonds may form through interactions between the amine groups in rhodamine B and oxygen-containing functional groups on the surfaces of both the composite and control materials. The C=C functional group of the aromatic ring in the composite is associated with the formation of $\pi-\pi$ interactions [8], whereas the Si-O-Si group resulting from the addition of silica to biochar enables $n-\pi$ interactions with rhodamine B [32]. Figure 9 provides an estimation of the interactions occurring between the composite and rhodamine B.

4. Conclusion

The silica-biochar composite derived from red mud and empty oil palm fruit bunches proves effective as an adsorbent for rhodamine B dye. The composite surface consists of functional groups such as -OH, C=O, C=C, C- O, C-H, and Si-O-Si and exhibits a larger surface area compared to silica (69.824 m^2/g) and biochar (95.452 m^2/g). The maximum amount of rhodamine B adsorbed was observed in the 1:2 (%w/w) variation of the composite, achieving 1.550 mg/g with an adsorption efficiency of 88.463%.

References

[1] Minh Duc Hoang, Quang Minh Do, Van Quang Le, Effect of curing regime on properties of red mud based alkali activated materials, *Construction and Building Materials*, 259, (2020), 119779 https://doi.org/10.1016/j.conbuildmat.2020.119779

[2] Zhanghong Wang, Dekui Shen, Fei Shen, Chunfei Wu, Sai Gu, Kinetics, equilibrium and thermodynamics studies on biosorption of Rhodamine B from aqueous solution by earthworm manure derived biochar, *International Biodeterioration & Biodegradation*, 120, (2017), 104-114 https://doi.org/10.1016/j.ibiod.2017.01.026

[3] Munir Ahmad, Adel R. A. Usman, Muhammad Imran Rafique, Mohammad I. Al-Wabel, Engineered biochar composites with zeolite, silica, and nano-zerovalent iron for the efficient scavenging of chlortetracycline from aqueous solutions, *Environmental Science and Pollution Research*, 26, 15, (2019), 15136-15152 https://doi.org/10.1007/s11356-019-04850-7

[4] Yu-Ying Wang, Hao-Hao Lu, Yu-Xue Liu, Sheng-Mao Yang, Removal of phosphate from aqueous solution by SiO_2–biochar nanocomposites prepared by pyrolysis of vermiculite treated algal biomass, *RSC Advances*, 6, 87, (2016), 83534-83546 https://doi.org/10.1039/C6RA15532D

[5] Kaifeng Wang, Na Peng, Jianteng Sun, Guining Lu, Meiqin Chen, Fucai Deng, Rongni Dou, Lijun Nie, Yongming Zhong, Synthesis of silica-composited biochars from alkali-fused fly ash and agricultural wastes for enhanced adsorption of methylene blue, *Science of The Total Environment*, 729, (2020), 139055 https://doi.org/10.1016/j.scitotenv.2020.139055

[6] Jianlong Wang, Shizong Wang, Preparation, modification and environmental application of biochar: A review, *Journal of Cleaner Production*, 227, (2019), 1002-1022 https://doi.org/10.1016/j.jclepro.2019.04.282

[7] Zhendong Zhao, Tiantian Nie, Wenjun Zhou, Enhanced biochar stabilities and adsorption properties for tetracycline by synthesizing silica-composited biochar, *Environmental Pollution*, 254, (2019), 113015 https://doi.org/10.1016/j.envpol.2019.113015

[8] Wen Huang, Min Zhang, Yinhai Wang, Jiao Chen, Jianqiang Zhang, Biochars prepared from rabbit manure for the adsorption of rhodamine B and Congo red: characterisation, kinetics, isotherms and thermodynamic studies, *Water Science and Technology*, 81, 3, (2020), 436-444 https://doi.org/10.2166/wst.2020.100

[9] Edi Sukirno, Anis Shofiyani, Nurlina, Pembuatan Membran Komposit Si/PVA/PEG Berbahan Dasar Silika Batu Padas Singkup Untuk Menurunkan Konsentrasi Ion Fosfat Dalam Larutan, *Jurnal Kimia Khatulistiwa*, 6, 4, (2017), 1-9

[10] Tri Ana Mulyati, Preparasi dan karakterisasi karbon aktif dari limbah ampas tebu menggunakan aktivator KOH, *Indonesian Chemistry Application Journal*, 1, 2, (2017), 61-67 https://doi.org/10.26740/icaj.v1n2.p61-67

[11] Haryono, Atiek Rostika Noviyanti, Engela Evy Ernawati, Sintesis, Karakterisasi, dan Uji Adsorpsi Komposit Silika/Karbon dari Limbah Sekam Padi sebagai Adsorben Tembaga (II), *Jurnal Teknologi Lingkungan*, 24, 1, (2023), 058-066 https://doi.org/10.55981/jtl.2023.241

[12] S. Salamah, W. Trisunaryanti, I. Kartini, S. Purwono, Synthesis and characterization of mesoporous silica from beach sands as silica source, *IOP Conference Series: Materials Science and Engineering*, 1053, 1, (2021), 012027 https://doi.org/10.1088/1757-899X/1053/1/012027

[13] Arnaldo Ramírez, Leonir Gómez, Alejandro J. Müller, Blanca Rojas de Gáscue, Characterization and Modification of Red Mud and Ferrosilicomanganese Fines and Their Application in the Synthesis of Hybrid Hydrogels, *Polymers*, 14, 20, (2022), 4330 https://doi.org/10.3390/polym14204330

[14] M. N. A. Uda, Subash C. B. Gopinath, Uda Hashim, N. H. Halim, N. A. Parmin, M. N. Afnan Uda, Periasamy Anbu, Production and characterization of silica nanoparticles from fly ash: conversion of agro-waste into resource, *Preparative Biochemistry & Biotechnology*, 51, 1, (2021), 86-95 https://doi.org/10.1080/10826068.2020.1793174

[15] Sara Ahmed, Tao Meng, Mazahir Taha, Utilization of red mud for producing a high strength binder by composition optimization and nano strengthening, *Nanotechnology Reviews*, 9, 1, (2020), 396-409 https://doi.org/10.1515/ntrev-2020-0029

[16] Yaguang Wang, Xiaoming Liu, Yong Li, Dongsheng Li, Wei Zhang, Yang Xue, Tailings after Iron Extraction in Bayer Red Mud by Biomass Reduction: Pozzolanic Activity and Hydration Characteristics, *Materials*, 14, 14, (2021), 3955 https://doi.org/10.3390/ma14143955

[17] Lichao Feng, Wenliang Yao, Kai Zheng, Na Cui, Ning Xie, Synergistically Using Bauxite Residue (Red Mud) and Other Solid Wastes to Manufacture Eco-Friendly Cementitious Materials, *Buildings*, 12, 2, (2022), 117 https://doi.org/10.3390/buildings12020117

[18] Smita Singh, M. U. Aswath, Rahul Das Biswas, R. V. Ranganath, Harish K. Choudhary, Rajeev Kumar, Balaram Sahoo, Role of iron in the enhanced reactivity of pulverized Red mud: Analysis by Mössbauer spectroscopy and FTIR spectroscopy, *Case Studies in Construction Materials*, 11, (2019), e00266 https://doi.org/10.1016/j.cscm.2019.e00266

[19] Noor-ul Amin, Safeena Khattak, Shahista Noor, Inayat Ferroze, Synthesis and characterization of silica from bottom ash of sugar industry, *Journal of Cleaner Production*, 117, (2016), 207-211 https://doi.org/10.1016/j.jclepro.2016.01.042

[20] P. R. Yaashikaa, P. Senthil Kumar, Sunita J. Varjani, A. Saravanan, Advances in production and application of biochar from lignocellulosic feedstocks for remediation of environmental pollutants, *Bioresource Technology*, 292, (2019), 122030 https://doi.org/10.1016/j.biortech.2019.122030

[21] M. Napitupulu, D. K. Walanda, M. Simatupang, Utilization of red fruit's peel (*freycinetia arborea gaudich*) as biochar for lead (Pb) adsorption, *Journal of Physics: Conference Series*, 1434, (2020), 012033 https://doi.org/10.1088/1742-6596/1434/1/012033

[22] Norazlina Abu Sari, Che Fauziah Ishak, Rosenani Abu Bakar, Characterization of Oil Palm Empty Fruit Bunch and Rice Husk Biochars and Their Potential to Adsorb Arsenic and Cadmium, *American Journal of Agricultural and Biological Sciences*, 9, 3, (2014), 450-456 https://doi.org/10.3844/ajabssp.2014.450.456

[23] Nurul Suraya Rosli, Shuhaida Harun, Jamaliah Md Jahim, Rizafizah Othaman, Chemical and physical characterization of oil palm empty fruit bunch, *Malaysian Journal of Analytical Sciences*, 21, 1, (2017), 188-196 http://dx.doi.org/10.17576/mjas-2017-2101-22

[24] Stasha Eleanor Rosland Abel, Soh Kheang Loh, Noorshamsiana Abdul Wahab, Ondrej Masek, Musa Idris Tanimu, Robert Thomas Bachmann, Effect of operating temperature on physicochemical properties of empty fruit bunch cellulose-derived biochar, *Journal of Oil Palm Research*, 33, 4, (2021), 643-652 https://doi.org/10.21894/jopr.2021.0007

[25] Liqiang Zhang, Zhengda Yang, Shanshan Li, Xinwei Wang, Riyi Lin, Comparative study on the two-step pyrolysis of different lignocellulosic biomass: Effects of components, *Journal of Analytical and Applied Pyrolysis*, 152, (2020), 104966 https://doi.org/10.1016/j.jaap.2020.104966

[26] Dengyu Chen, Kehui Cen, Xiaozhuang Zhuang, Ziyu Gan, Jianbin Zhou, Yimeng Zhang, Hong Zhang, Insight into biomass pyrolysis mechanism based on cellulose, hemicellulose, and lignin: Evolution of volatiles and kinetics, elucidation of reaction pathways, and characterization of gas, biochar and bio - oil, *Combustion and Flame*, 242, (2022), 112142 https://doi.org/10.1016/j.combustflame.2022.112142

[27] Ahmad Fitriansyah, Hermansyah Amir, Elvinawati Elvinawati, Karakterisasi Adsorben Karbon Aktif dari Sabut Pinang (*Areca catechu*) Terhadap Kapasitas Adsorpsi Zat Warna Indigosol Blue 04-B, *ALOTROP*, 5, 1, (2021), 42-54 https://doi.org/10.33369/atp.v5i1.16485

[28] Munir Ahmad, Mahtab Ahmad, Adel R. A. Usman, Abdullah S. Al-Faraj, Adel Abduljabbar, Yong Sik Ok, Mohammad I. Al-Wabel, Date palm waste-derived biochar composites with silica and zeolite: synthesis, characterization and implication for carbon stability and recalcitrant potential, *Environmental Geochemistry and Health*, 41, 4, (2019), 1687-1704 https://doi.org/10.1007/s10653-017-9947-0

[29] Jianhua Guo, Baoliang Chen, Insights on the Molecular Mechanism for the Recalcitrance of Biochars: Interactive Effects of Carbon and Silicon Components, *Environmental Science & Technology*, 48, 16, (2014), 9103-9112 https://doi.org/10.1021/es405647e

[30] Adhi Setiawan, Achmad Fatoni, Tarikh Azis Ramadani, Pemurnian Bioetanol Menggunakan Adsorben Silika Gel dari Limbah Botol Kaca di Industri Kecap, *Jurnal Pengendalian Pencemaran Lingkungan*, 4, 2, (2022), 74-83 https://doi.org/10.35970/jppl.v4i2.1435

[31] J. Anandkumar, B. Mandal, Adsorption of chromium(VI) and Rhodamine B by surface modified tannery waste: Kinetic, mechanistic and

thermodynamic studies, *Journal of Hazardous Materials*, 186, 2, (2011), 1088-1096 https://doi.org/10.1016/j.jhazmat.2010.11.104

[32] Yao Zhu, Baojun Yi, Qiaoxia Yuan, Yunlian Wu, Ming Wang, Shuiping Yan, Removal of methylene blue from aqueous solution by cattle manure-derived low temperature biochar, *RSC Advances*, 8, 36, (2018), 19917-19929 https://doi.org/10.1039/C8RA03018A